Biosensors and Bioelectronics 124–125 (2019) 167–175

Contents lists available at ScienceDirect

Biosensors and Bioelectronics

journal homepage: www.elsevier.com/locate/bios

Molecularly-imprinted chloramphenicol sensor with laser-induced graphene electrodes

Ana R. Cardoso[a,b,1], Ana C. Marques[a,b,1], Lídia Santos[b,c], Alexandre F. Carvalho[b,d], Florinda M. Costa[d], Rodrigo Martins[b], M. Goreti F. Sales[a,*], Elvira Fortunato[b,**]

[a] BioMark/Centro de Engenharia Biológica (Universidade do Minho), in Instituto Superior de Engenharia do Porto, R. Dr. António Bernardino de Almeida, 431, 4200-072 Porto, Portugal
[b] i3N/CENIMAT, Department of Materials Science, Faculty of Science and Technology, Universidade NOVA de Lisboa and CEMOP/UNINOVA, Campus de Caparica, 2829-516 Caparica, Portugal
[c] Hovione, Campus do Lumiar, Edifício S, Estrada do Paço do Lumiar, 1649-038 Lisboa, Portugal
[d] i3N/Department of Physics, Universidade de Aveiro, Campus Universitário de Santiago, Aveiro 3810-193, Portugal

ARTICLE INFO

Keywords:
Laser irradiation
On-site graphene production
Three-electrode system
Molecularly-imprinted polymer
Chloramphenicol

ABSTRACT

Graphene has emerged as a novel material with enhanced electrical and structural properties that can be used for a multitude of applications from super-capacitors to biosensors. In this context, an ultra-sensitive biosensor was developed using a low-cost, simple and mask-free method based on laser-induced graphene technique for electrodes patterning. The graphene was produced on a polyimide substrate, showing a porous multi-layer structure with a resistivity of $102.4 \pm 7.3\,\Omega$/square. The biosensor was designed as a 3-electrode system. Auxiliary and working electrodes were made of graphene by laser patterning and the reference electrode was handmade by casting a silver ink. A molecularly-imprinted polymer (MIP) was produced at the working electrode by direct electropolymerization of eriochrome black T (EBT). As proof-of-concept, the MIP film was tailored for chloramphenicol (CAP), a common contaminant in aquaculture.

The resulting device was evaluated by cyclic voltammetry and electrochemical impedance spectroscopy readings against a redox standard probe. The limit of detection (LOD) was 0.62 nM and the linear response ranged from 1 nM to 10 mM. These analytical features were better than those produced by assembling the same biorecognition element on commercial graphene- and carbon-based screen-printed electrodes.

Overall, the simplicity and quickness of the laser-induced graphene technique, along with the better analytical features obtained with the graphene-based electrodes, shows the potential to become a commercial approach for on-site sensing.

1. Introduction

In the last decades, the development of portable, low-cost and effective devices for analytical purposes has been widely increasing (Bernalte et al., 2016). Among the different analytical techniques, electrochemical biosensors have received large interest due to their high sensitivity and selectivity, easy miniaturization, low instrumentation cost and rapid and simple results (Arduini et al., 2016; Bernalte et al., 2016; Hayat and Marty, 2014; Taleat et al., 2014). The highest icon of these electrochemical devices is the glucose meter, including glucose strips that combine in the same spot (small size) two or three electrodes and allow glucose monitoring with a small drop of blood, in point-of-care (Yamanaka et al., 2016; Yoo and Lee, 2010).

The great advances generated by the glucose meters are an outcome of miniaturization, in which the multiple electrode-system is small, standing in a close and fixed position. This configuration offers many analytical advantages, such as the ability to measure small currents in the range of pA to nA, rapid response to changes in applied potential, low ohmic reduction in electric potential, efficient diffusional mass transport, and steady-state response at diffusion controlled potential, while requiring very low sample volumes (Rackus et al., 2015).

The commercial versions of combined electrode systems are typically based on carbon, an easily available and low-cost material, with good electrical properties. Carbon-based materials, especially carbon

---

[*] Correspondence to: School of Engineering of the Polytechnique School of Porto, R. Dr. António Bernardino de Almeida, 431, 4200-072 Porto, Portugal.
[**] Correspondence to: CENIMAT/i3N, Faculdade de Ciências e Tecnologia, Campus da Caparica, 2829-516 Caparica, Portugal.
E-mail addresses: mgf@isep.ipp.pt (M.G.F. Sales), emf@fct.unl.pt (E. Fortunato).
[1] Equal first authors.

https://doi.org/10.1016/j.bios.2018.10.015
Received 3 September 2018; Accepted 9 October 2018
Available online 14 October 2018

nanotubes or graphene, have revolutionized the scope of commercial screen-printed electrodes in electro-analysis. The electrochemical properties of carbon nanostructures, such as faster electron transfer kinetics, low residual current, readily renewable surface and wide potential window renders carbon-based nanostructures as promising candidates for biosensing applications, in comparison to other carbon-based electrode materials like glassy carbon (Ramnani et al., 2016). Graphene, in particular, is a promising material due to its unique properties like an extraordinary electron transfer capability and excellent thermal conductivity (Kim et al., 2015; Kumar et al., 2015; Song et al., 2016; Trojanowicz, 2016; Zheng et al., 2015).

The carbon-based electrochemical devices available in the market are normally fabricated by lithography or screen-printing techniques, on top of ceramic substrates. However, these devices require sometimes complex processes rendering expensive and time-consuming production procedures, thus making these commercial devices expensive (Chang et al., 2016). Overall, the development and application of one-step, scalable and versatile approaches to produce carbon-based electrodes patterning is essential.

Recently, Lin et al. (2014) reported a one-step and novel technique termed laser-induced graphene (LIG) which enables the modification of a polyimide substrate into a 3D porous graphene structure, exhibiting high electrical conductivity. This one-step process allows patterning porous graphene films with a surface area of ~ 340 m^2/g, comparable to that of the wet-chemistry derived 3D graphene (Lin et al., 2014), using a CO_2 infrared laser without using high temperature processes, solvents or subsequent treatments, that photothermally convert sp^3-carbon atoms into sp^2-carbon atoms by pulsed laser irradiation. The energy from the laser irradiation results in lattice vibrations, rendering high localized temperatures, thus breaking the C–O, C=O and N–C bonds. Lastly, the aromatic compounds rearranged themselves to form graphitic structures. This new method for graphene production has already been used for some applications, such as capacitors, biosensors, among others (Cai et al., 2016; Chyan et al., 2018; El-Kady et al., 2012; Fenzl et al., 2017; In et al., 2015; Luo et al., 2016; Tehrani and Bavarian, 2016; Xu et al., 2018; Ye et al., 2018). The overall composition of graphene depends on the polymer substrate and on the experimental conditions selected, rendering multi layered graphene. Fig. 1 explains the main process of the graphene formation using the LIG process. This is a similar process to what happens to silicon oxide formation by thermal oxidation of silicon, where part of the pristine material is converted into another one.

Herein, a 3-electrode system produced by laser irradiation on a polyimide substrate applied to the production of a biosensor using a molecularly-imprinted material as biorecognition element is presented for the first time. As proof-of-concept, chloramphenicol (CAP), an antibiotic found in the aquatic environment, was selected as target compound. CAP is a broad-spectrum antibiotic effective against many bacteria (Cardoso et al., 2018). This antibiotic can be detected by several methods, such as high-performance liquid chromatography (HPLC) alone or combined with mass spectroscopy (HPLC-MS), gas chromatography (GC), and enzyme-linked immunosorbent assay (ELISA) (Zhou et al., 2015). However, these methods are complex, time-consuming, expensive and the level of quantification may not be low enough to meet the minimum required performance limit of 0.3 g kg^{-1}, for CAP residues in food products of animal origin, established by the European Commission (Abnous et al., 2016; Ashwin et al., 2005). So, the development of a biosensor presents several advantages when compared to the conventional methods, such as more sensitive, faster, more accurate and easier readings (Samsonova et al., 2012; Xia et al., 2013).

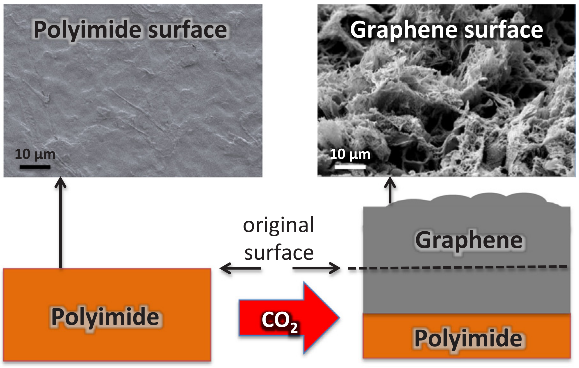

Fig. 1. Schematic of the graphene formation using the LIG process.

The biorecognition element was produced on-site, by direct electropolymerization of a suitable monomer (Cardoso et al., 2018), thereby anticipating the implementation of industrial processes in a larger scale. The overall conditions to yield the best carbon material on the polyimide substrate were studied and optimized. The overall analytical features of the biosensor assembled on the LIG-based devices are compared to those generated by screen-printed (SPE) commercial devices with three-carbon electrode systems, with carbon (C-SPE) and graphene (G-SPE) electrodes.

2. Experimental section

2.1. Reagents and solutions

During this work, ultrapure Milli-Q water laboratory grade (conductivity $^{<}$0.1µS/cm) was used to prepare all solutions. The chemical reagents including potassium hexacyanoferrate III ($K_3[Fe(CN)_6]$) and potassium hexacyanoferrate II ($K_4[Fe(CN)_6]$) trihydrate, were purchased from Riedel-de Häen; potassium chloride (KCl) from Merck; acetonitrile (ACN) and ethanol absolute from Carlo Erba; 3,4-ethylenedioxythiophene, 97% (EDOT) from Alfa Aesar; 4-aminothiophenol, 96% (4-AMP) from Acros Organics; eriochrome black T (EBT) from Biochem; chloramphenicol (CAP) and oxytetracycline (OTC) from Fluka; sodium sulfadiazine, amoxicillin (AMC) and lithium perchlorate, from Sigma Aldrich.

2.2. Device fabrication

The LIG-based device architecture was designed as a 3-electrode configuration (counter, working and reference electrode, named CE, WE, RE, respectively) using a vector image software (Adobe illustrator, Adobe systems software, Ireland). CE and WE were engraved on a polyimide (PI) substrate (Dupont, 0.075 mm of thickness) to LIG, on a computer controlled – CO_2 laser machine (VLS 3.50, Universal laser systems), with a 10.6 µm wavelength and a beam size of 0.127 mm diameter, at different power (from 5 to 37.5 W) and speeds (3.4, 6.8 and 10.2 cm/s), at 1000 ppi (pulses per inch) (Table S1), to obtain the highest quality product. Silver conductive ink (AG-510 silver ink, surface resistivity: < 0.015 Ω/square/mil, Conductive Compounds, Inc., New Hampshire, USA) was used to define the reference electrode and the conductivity tracks, followed by a curing process in a hot plate (120 °C, 10 min). The devices were then encapsulated on plastic sheets using a home version laminator. The plastic sheets were previously patterned, in the CO_2 laser machine, to define the electrodes and electrical tracks area. Lastly, the devices were individualized to a dimension of 1.0 × 2.5 cm^2 (Fig. 2).

2.2.1. Electrodes characterization

The synthesized carbonaceous material trough photothermally conversion of a polyimide substrate by laser irradiation was further characterized by Scanning Electron Microscopy (SEM), Micro-Raman Spectroscopy, X-rays Diffraction (XRD) and Hall effect.

SEM (Carl Zeiss AURIGA Crossbeam SEM-FIB, Oberkochen, Germany) was used to assess the morphology of the 3D network LIG.

Micro-Raman spectroscopy was carried out using a blue line

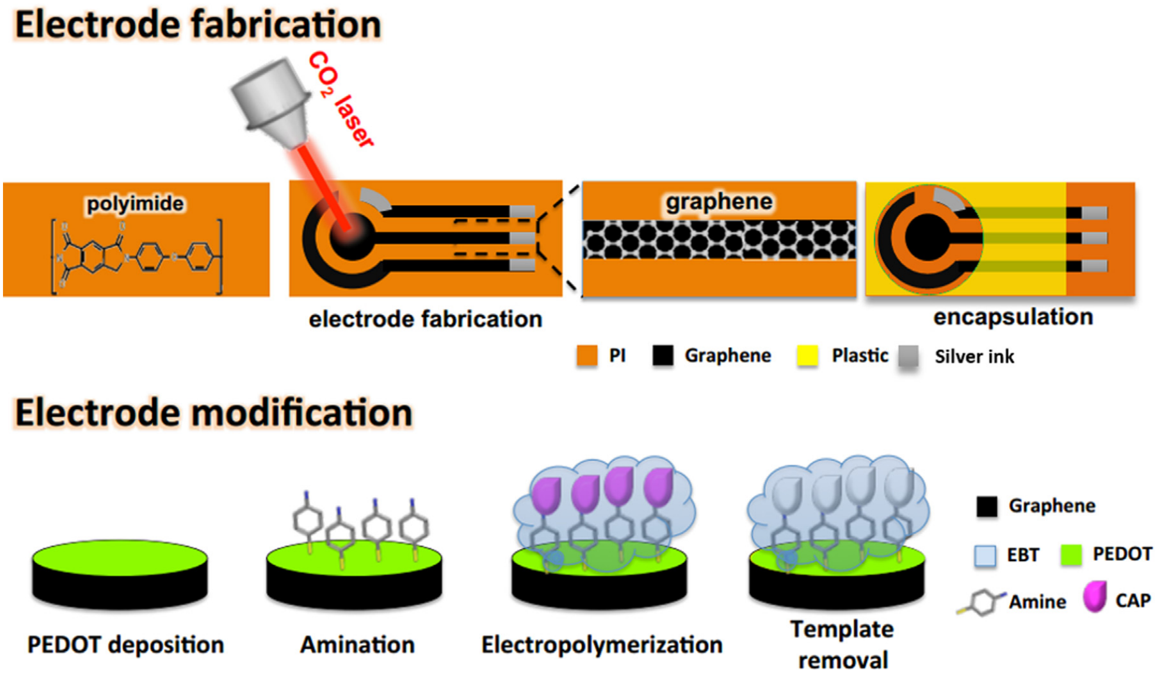

Fig. 2. Schematic representation of the workflow employed on the production of the LIG electrodes (top) and the MIP fabrication (bottom) for the electrochemical biosensor for detection of CAP (electrodeposition of EDOT with subsequent formation of poly(EDOT), followed by amination, electropolymerization of EBT, in the presence of CAP (MIP) or without CAP (NIP), and finally template removal).

(442 nm) excitation from a He:Cd laser, using a Jobin Yvon T64000 equipment in the backscattering configuration. The spectra were collected from several regions of different samples, processed under distinct experimental conditions.

XRD (X'Pert Pro, PANalytical, Almelo, Netherlands) was performed with CuKα target and wavelength of 1.5406 Å from 10° to 70°. The diffractogram was obtained for LIG in powder form.

Lastly, the electrical sheet resistance (Ω/square), was determined by Hall effect measurements in Van der Pauw geometry in a Biorad HL 5500 equipment using a constant magnetic field of 0.5 T at room temperature. These measurements were performed for all LIG samples.

2.3. *Electrochemical biosensor fabrication on commercial and LIG devices*

The biosensor was fabricated through molecular imprinting polymer technique, following a previous work of the authors (Cardoso et al., 2018). The fabrication was performed in commercial screen-printed devices (carbon/graphene) and in the LIG device. The assembly process was similar for all devices, except for the one step that was only performed for the LIG device. First, the LIG WE was stabilized and modified to be able to receive the MIP sensing layer. For this purpose, the as-produced LIG devices were incubated in 0.01 M EDOT in 0.10 M KCl (180 s), to fix some loosen LIG particles created during laser irradiation, and to render a higher homogeneous surface. After WE cleaning by chronoamperometry with 0.10 M KCl (180 s at 1.70 V), the surfaces were rinsed with ultrapure water to eliminate residual chemical compounds. Then EDOT was electrochemically polymerized in the electrode sensing area (10 s at 0.90 V), followed by incubation in 0.01 M 4-AMP (prepared in Milli-Q water and ethanol, 1:1) for 1 h, to ensure a covalent bonding to the PEDOT structure and to firmly attach to the surface the MIP layer. The MIP layer was produced by bulk electropolymerization of functional monomers (EBT) in the presence of the template CAP in ACN buffer (0.10 M CAP in 0.20 M ACN with 1.0×10^{-3} M of EBT in 0.20 M ACN), while the NIP layer was produced without the CAP by chronoamperometry (250 s at 0.95 V). After assembling the MIP film, the CAP template was removed by incubating the sensing layer in ACN and performing consecutive CV scanning from − 0.2 to 0.8 V, with a scan-rate of 0.1 V/s for 20 cycles. This potential range was selected to maintain the integrity of the polymer while avoiding the electro-activity of CAP, which could irreversibly entrap the template within the polyEBT film (Fig. 2).

2.3.1. *Electrochemical measurements and procedures*

The electrochemical measurements were performed with a potentiostat/galvanostat from Metrohm Autolab, PGSTAT320N, controlled by NOVA 1.11 software. The graphene screen printed electrodes (G-SPEs) and carbon screen printed electrodes (C-SPEs) were purchased from ORION. The screen printed commercial devices, as well as the produced LIG device had a 3-electrode configuration architecture, with a 4.0 mm diameter WE. All devices were interfaced in a switch box from BioTID Electronica, to perform the electrochemical assays.

All electrochemical assays were carried out in duplicate. Cyclic voltammetry (CV) assays were carried out from − 0.3 to + 0.7 V, at a scan-rate of 50 mV/s. Electrochemical Impedance Spectroscopy (EIS) assays were performed at an open circuit potential, using a sinusoidal potential perturbation with an amplitude of 0.01 V, and 50 data points, logarithmically distributed over 10–0.01 Hz frequency range. The EIS data was fitted into a Randles equivalent circuit, using 1.11 Nova Software from Autolab.

The electrical properties of the modified surfaces were followed-up by CV and EIS assays, carried out with a redox probe solution of 5.0×10^{-3} M $[Fe(CN)_6]^{3-}$ and 5.0×10^{-3} M $[Fe(CN)_6]^{4-}$, prepared in 0.20 M ACN buffer. Calibration curves were followed by EIS with standard solutions of CAP prepared in lithium perchlorate buffer (ranging from 1.0 nM to 10 mM), within the same linear range. The LOD corresponded to the signal $X + 3\sigma$, where X represents the average value of the EIS blank signals (obtained in the absence of CAP) and σ is the known standard deviation of EIS blank signal consecutive readings (Harvey, 2000).

Selectivity studies were made as previously reported (Cardoso et al., 2018). In detail, the concentration of CAP and interfering species was set to 1.00×10^{-6} M. Four independent biosensors were used for this purpose. The first sensor was incubated in CAP alone and the others were incubated with mixed solution (CAP and each interfering specie).

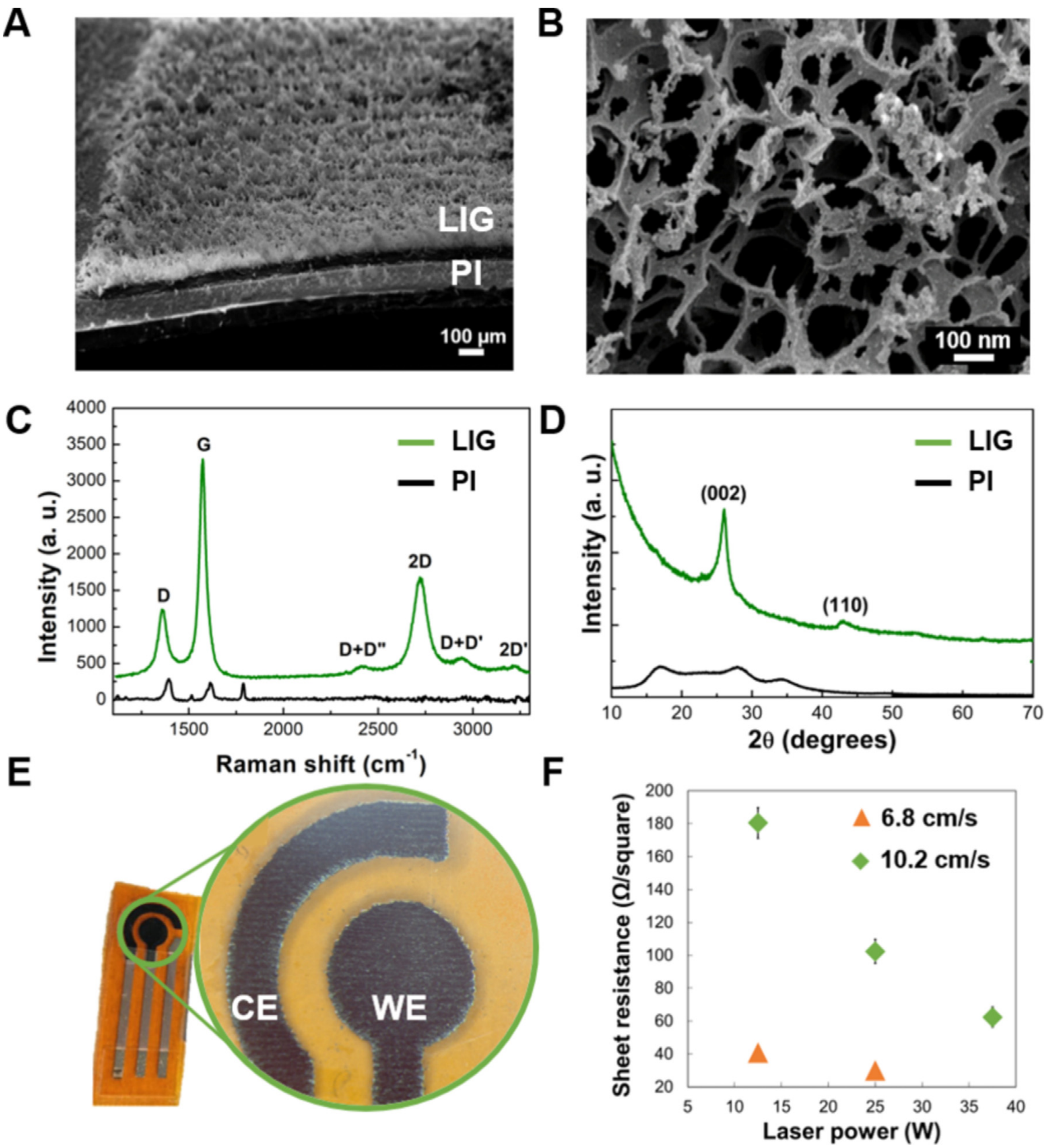

Fig. 3. Electrodes characterization: SEM images of (**A**) the lateral view of laser-induce graphene (LIG) on top of polyimide (PI) and (**B**) Amplified SEM image of LIG surface; (**C**) Raman spectra and (**D**) XRD diffractogram of LIG sample and PI substrate; (**E**) Real image of the device with an amplification of the working and counter LIG electrodes; (**F**) Sheet resistance, calculated by Hall effect, for the fives samples (n = 4) produced with different laser power and speed.

The incubation time was set to 20 min (the same as in the calibration with only CAP). As interfering species, other antibiotics used in fish farming were tested, namely oxytetracycline (OTC), amoxicillin (AMC) and sulfadiazine.

3. Results and discussion

3.1. Electrodes production

A CO_2 infrared laser was used to photothermally convert a polyimide (PI) substrate into a carbon matrix, mostly composed by graphene. The patterning of 2.0 cm^2 squares on PI substrate was tested with a laser speed of 3.4, 6.8 and 10.2 cm/s and a laser power of 5, 12.5, 25 and 37.5 W (Table S1). Overall, no graphene formation was observed at 5 W for the selected speeds, while at 12.5 W and 25 W a total conversion into graphene was achieved for 6.8 and 10.2 cm/s speeds. With 37.5 W laser power, the conversion to graphene only occurred at the higher speed. Therefore, only five samples were eligible for characterization (Fig. 3).

The SEM images (Fig. 3A, B) showed a foamy-like appearance, with a layer on the PI surface of approximately 100 µm of thickness (Fig. 3A), and a porous 3D network (Fig. 3B), resulting from the rapid liberation of gaseous products (Lin et al., 2014). The porous structure presented variable dimensions. The smaller dimension porous diameter was calculated to be roughly 256 nm with 144 nm as standard deviation, showing little uniformity. Nevertheless, this porous structure rendered a high surface area which can enhance their performance as sensor devices, as well as for other applications like wastewater remediation, supercapacitors, fuel cells, among others (Lin et al., 2014; Ma and Chen, 2015; Xu et al., 2017; Żelechowska et al., 2014).

The starting PI material was characterized by Raman spectroscopy (Fig. 3C) showing a set of features commonly found in the literature

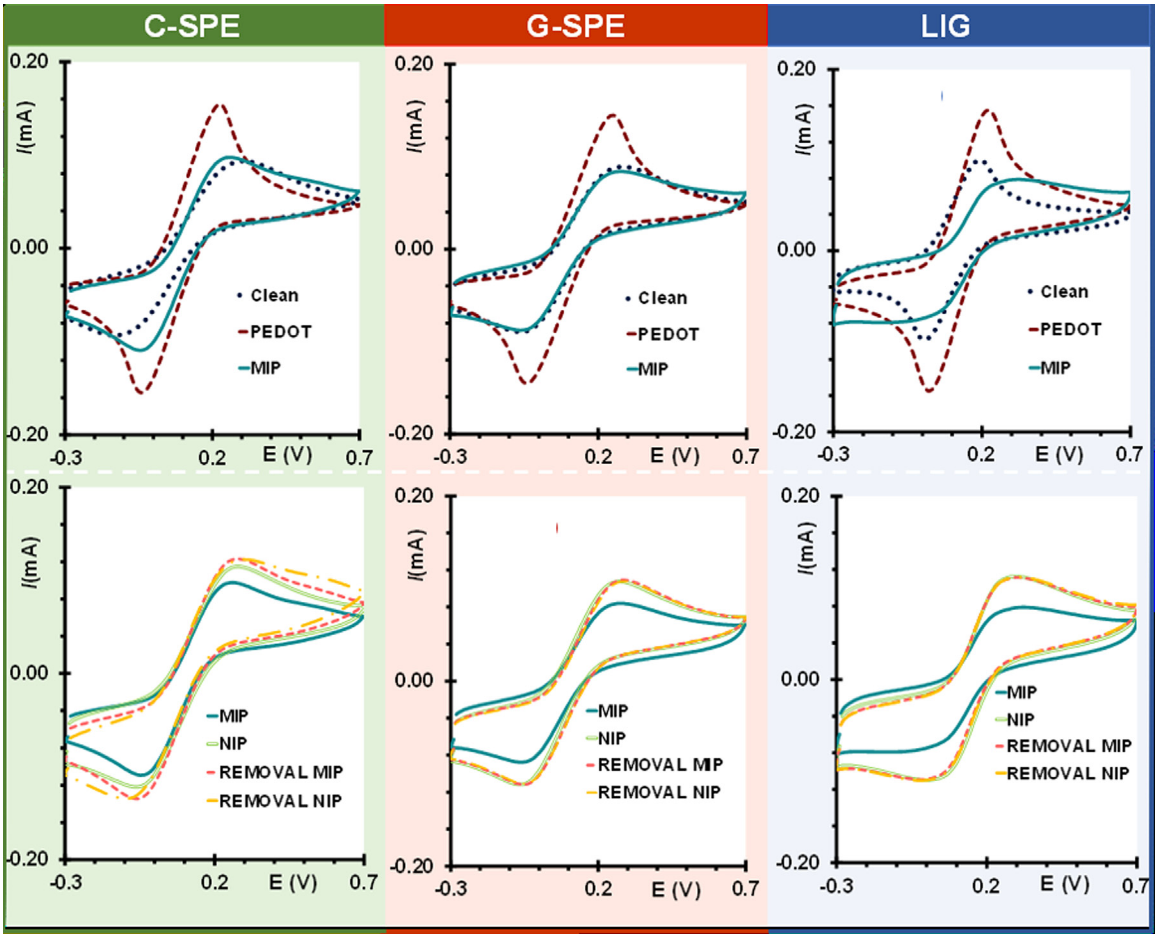

Fig. 4. Voltammograms of the C-SPE, G-SPE and LIG-based sensors, scanned in a solution of 5.0×10^{-3} M $[Fe(CN)_6]^{3-/4-}$ prepared in buffer/ACN, after different stages of surface modification.

(Yang et al., 2013). C-N-C transverse and axial vibrations occur at 1125 and 1395 cm^{-1}, respectively, C=C stretch at 1515 cm^{-1}, carboxylic acid at 1598 cm^{-1} (shoulder), aromatic imide at 1615 cm^{-1}, and C=O symmetric stretch at 1787 cm^{-1}. No polyimide Raman signal was found in LIG, suggesting a full conversion at the surface. The normalization of the Raman spectra to the G-band (1573 cm^{-1}) revealed that all samples were uniform and similar to each other. Fig. 2C shows a representative spectrum of the sample achieved with the optimized conditions (25 W at 10.22 cm/s) used to produce the biosensor structural layer, exhibiting the typical signature of a graphene foam sample, and featuring wide and intense D, G and 2D bands (Lin et al., 2014). The presence of the defect-allowed D band at 1362 cm^{-1}, corresponding to the breathing mode of sp^2 coordinated 6 atom rings in defective graphitic phases, suggests a moderate density of lattice defects, activating the D band, forbidden in perfect graphene due to momentum conservation selection rules (Carvalho et al., 2016). These defects are also present at the edges of graphene sheets, which appear in great quantities in graphene foams. Furthermore, the presence of covalently bonded oxygen, typical of LIG, provides local defects that induce the Raman D band (Lin et al., 2014). The broadening of the D band to 51 cm^{-1} full width at half maximum is due to phonon scattering at defects. The prominent G band corresponds to the stretching mode of the sp^2 C-C bonds. The 2D band (2722 cm^{-1}), a second-order two phonon process, sometimes referred to as an overtone of the D band, is the result of a two-phonon lattice vibrational process. The defect-allowed D band exhibits a high intensity, with an I_G/I_D ratio of 3.5, suggesting defective graphene. Moreover, the I_{2D}/I_G ratio (0.44) suggests a multi-layered nature of the graphene foams. However, the perfect fit with a single Lorentzian curve hints that there is weak coupling between graphene sheets (Rao et al., 2011). The D + D″, D + D′ and 2D′ bands are also typical of graphene and graphene-based materials (Ferrari and Basko, 2013). Out of those, the D + D′ (often identified as D + G) band is also present in defective graphene structures (Ferrari and Basko, 2013; Lin et al., 2014). The typical Raman spectra obtained is compatible with graphene foams produced by the interaction of a laser beam with polyimide sheets (Lin et al., 2014), with a 2D band typically lower than the G band and an intense D band. The presence of defects can be beneficial for analytical purposes, since it has been demonstrated that electron transfer has higher rates on graphene edge-plane than in the basal plane (Li et al., 2011).

Fig. 2D puts in evidence the XRD diffractogram of PI, where a pattern of wide bands at low angles typical of this polymeric material is patent (Fang et al., 2016). The XRD diffractogram obtained for LIG in powder form shows an intense peak at 26.03°, attributed to the (002) plane, and a peak at 43.00° indexed to (110) reflections originated by an in-plane structure (Lin et al., 2014).

Hall effect measurements were carried out for all five LIG materials, to determine the sheet resistance (Fig. 3F) and choose the proper conditions for the device production. The lowest LIG sheet resistance, of 30.0 ± 2.6 Ω/square, was obtained at 6.82 cm/s with 25 W. However, the combination of low speed and medium power lead to PI substrates that started increasingly heating during laser irradiation and created holes and/or overly loose graphene powder on the PI substrate when large areas were patterned. For this reason, the optimized power and speed of the CO_2 laser was considered 25 W and 10.22 cm/s, yielding a relative low sheet resistance of 102.4 ± 7.3 Ω/square and larger patterned areas without defects on the electrodes (Fig. 3E).

The thermal analysis of the PI substrate (Fig. S1) was performed to ensure that the material could withstand the encapsulation and the Ag ink heating curing processes at 120 °C. The photothermal conversion of PI into graphene by laser irradiation allowed patterning of the electrodes, through consecutive scribing of horizontal lines (Fig. 3E), with a very low production time, approximately 15 s per sensor. This approach can be easily integrated in roll-to-roll processes, for a large-scale production. The resolution of the method was roughly 100 µm, thereby allowing freedom of design in the production of different sensor's geometries (Fig. S2), with high resolution, in an effective one-step approach.

3.2. Electrochemical characterization and comparison to commercial electrodes

Each chemical modification performed on the WE surface of C-SPE, G-SPE and LIG device was monitored by CV (Fig. 4) and EIS (Fig. S3) assays, following the changes in the electron transfer properties of the standard iron redox probe. The corresponding electrical data can be found in Tables S2 and S3.

In terms of CV, the currents of the clean electrodes were higher in the LIG-based sensors than in the commercial SPEs, a behaviour that was also being linked to a narrower peak-to-peak separation (Table S3). There were no significant differences between the clean C-SPEs and G-SPEs, but these were of commercial origin and it was not possible to infer the reason for this observation. In addition, the typical peak shape of the iron redox probe was well defined only in the LIG-based electrodes, thereby inferring the better electrical properties of these devices when compared to the commercial ones. In general, this distinct behaviour makes the LIG device a serious alternative candidate to the current commercially available SPEs.

With better electrical features in the blank signal, the subsequent electrochemical stages were also different for the LIG-based devices (Table S3). This was signalled in Fig. 4 by the lower peak-to-peak separation in the PEDOT film of LIG surfaces, although all substrates yielded similar current values after electropolymerization of EDOT (± 15 µA). The differentiated behaviour of LIG devices was also signalled by a higher amount of polymeric imprinted film formed. The formation of the imprinted polymer layer was revealed by the decreased currents of the redox peaks, in comparison with the PEDOT layer. The more the peak current decreased, the higher the amount of polymer formed on the surface. Considering that the PEDOT currents were higher in the LIG devices, the electrical stimulus generating the polymer layer was stronger in these, thereby yielding a higher amount of polymer. As expected, this higher amount of polymer was coupled with a higher peak-to-peak potential separation (Hughes et al., 2016; Khan et al., 2016).

Regarding the device, the MIP layer showed lower peak currents and a higher separation of cathodic and anodic peaks when compared to the NIP layer. As this polymer was being formed by an electrical potential applied to the electrode surface, the presence of CAP hindered the polymer growth. Thus, a higher amount of polymer was formed on the NIP layer (where there was no CAP). Overall, a greater difference between NIP and MIP films was promoted by the LIG device, most probably due to the higher extent of film formed on this surface compared to the SPEs.

For the template removal, the MIP and NIP films were exposed to an aqueous ACN solution. When the NIP was in contact with ACN, the peak separation of the iron redox probe remained unaltered, because nothing was being removed from the surface. In contrast, the extraction of CAP from the MIP network was evidenced by an increased peak separation, due to the facilitated current flow caused by the absence of antibiotic. Overall, this removal step confirmed that the LIG device gave rise to major differences between MIP and NIP, thereby suggesting better results in terms of analytical features.

In addition to the previous findings, it was interesting to note that the LIG device had a closer behaviour to the G-SPE in the imprinting stage. After electropolymerization, the current of the MIP films in these devices was of ∼ 8 µA, against ∼ 11 µA in the C-SPEs. This is likely confirming the characterization of the material, where the presence of graphene dominated the carbon nanostructure generated by laser irradiation of polyimide.

The previous CV findings were confirmed by EIS assays, shown in Fig. S3. As expected, in the cleaning step the LIG device showed a different behaviour compared to the other devices, due to the EDOT incubation prior to the biosensor assembly. Being EDOT a conducting monomer, it contributed to the absence of the typical semicircle in EIS. After EDOT electropolymerization, the LIG devices showed a greater impact from the formation of a higher amount PEDOT, yielding lower Rct values in the subsequent stages of modification. Moreover, the MIP polymer had a lower charge transfer resistance (Rct) compared to the NIP, which was assigned to the presence of CAP in the MIP polymerization step, as previously explained. The larger difference before and after CAP removal was, once again, obtained with the LIG device. Finally, the Rct remained constant after the NIP removal stage but decreased in the MIP film. Overall, the Nyquist plots reported a similar behaviour to that reported by the previous CV measurements.

3.3. Analytical performance

The analytical performance of the different carbon-based devices (C-SPE, G-SPE and LIG device) was evaluated by incubating the WE area with increasing concentrations of CAP standard solutions. For this purpose, a drop of each CAP standard solution was incubated for 20 min, allowing CAP rebinding. After this, the electrode was washed and incubated with the standard iron redox probe, for electrical readings. The resulting calibration data plotted Rct against logarithm CAP concentration (Fig. 5A).

In general, EIS measurements showed that increasing concentrations of CAP increased the electrical resistance of the surface, as the diameter of the semicircles in the Nyquist plots increased. This was a common trend between commercial and LIG devices. C-SPE showed a linear behaviour between 1 nM and 100 µM, with an average slope of 103.71 Ω/decade, and a standard deviation of 2.70%. The G-SPE device calibration displayed a linear response in the range of 1 nM to 1 mM, with a slope value of 77 Ω/decade and a standard deviation of 1.42%. Finally, the LIG device showed the broadest linear behaviour from 1 nM to 10 mM with an average slope of 162.5 Ω/decade (higher than the commercial SPEs) and a standard deviation of 3.18%. The squared correlation coefficient of all calibrations was 0.99. The standard error ranged from 0.18% to 6.67%, with an average of 2.29%.

Overall, these results showed that all 3-electrode systems displayed a highly sensitive response for CAP determination. Yet, the LIG device described herein showed an increased performance, when compared to G-SPE or the C-SPE, considering sensitivity and extent of linear range. The slope of the LIG calibration represented 156% of the C-SPE slope and 209% of the G-SPE slope. The wider linear range was observed for the LIG-devices, with commercial SPE evidencing earlier signal saturation for the higher CAP concentrations. The limit of detection (LOD) of the LIG-based MIP biosensor was 0.62 nM.

In parallel, the same measurements were performed with the corresponding NIP devices, which serve as a control of the imprinting process, monitoring the non-specific response of the sensing film (Fig. 5B). In general, the results presented a random behaviour against increasing CAP concentrations in all devices. Overall, these results showed that the NIP film was unable to detect CAP, independently of its concentration, thus suggesting negligible non-specific interactions between CAP and poly(EBT).

To further assess the selectivity of the device, selectivity studies were made for LIG device, as in Cardoso et al. (2018). The results obtained are shown in Fig. 6, evidencing the relative standard deviation

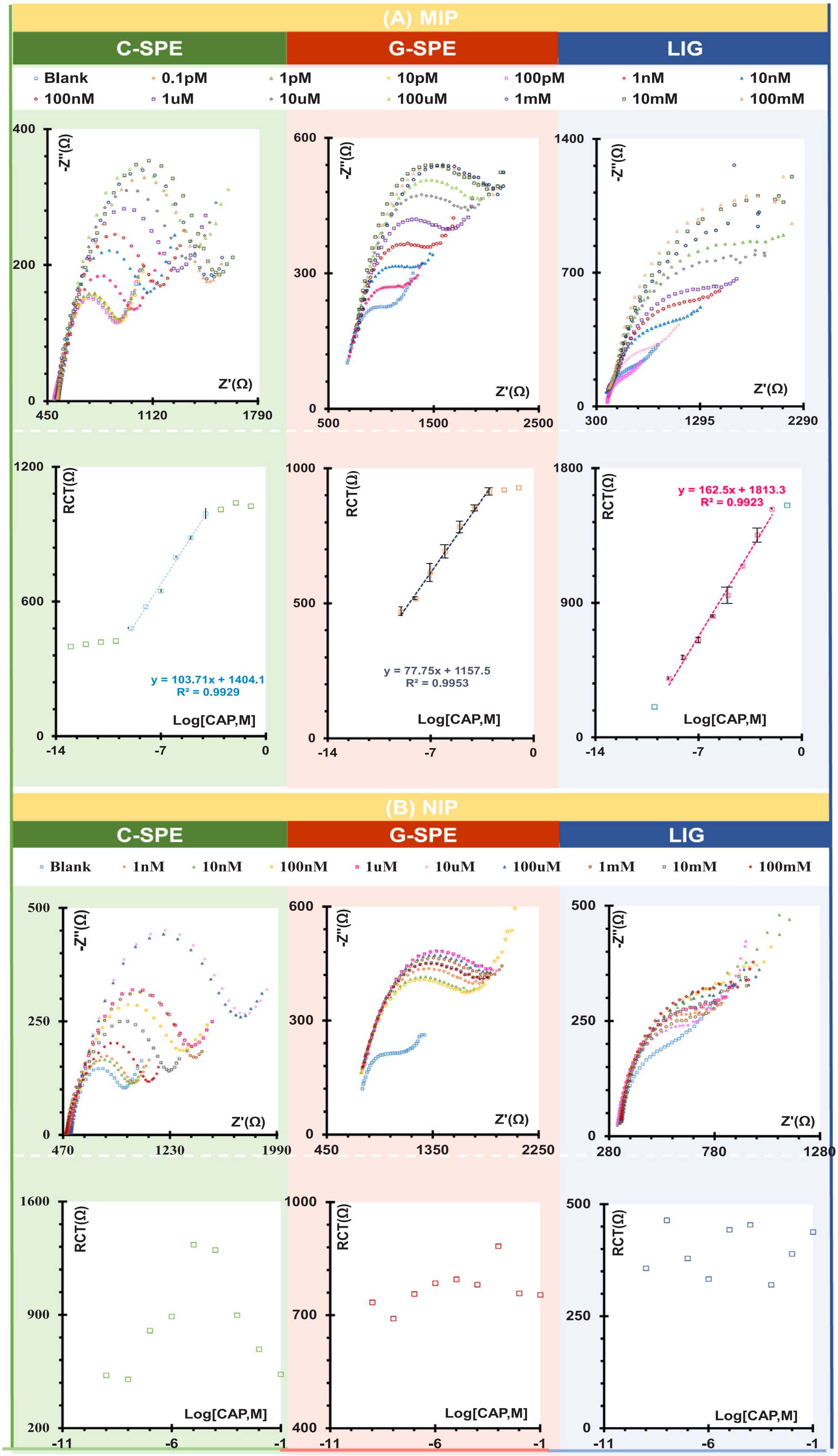

Fig. 5. **(A)** EIS measurements of MIP devices (top) and the corresponding calibration curves (bottom), obtained in 5.0 × 10^{-3} M $[Fe(CN)_6]^{3-}$ and 5.0 × 10^{-3} M $[Fe(CN)_6]^{4-}$ solution prepared in lithium perchlorate, after incubation in increasing concentrations of CAP standard solutions; **(B)** EIS measurements of NIP devices (top) and the corresponding calibration curves (bottom), obtained in 5.0 × 10^{-3} M $[Fe(CN)_6]^{3-}$ and 5.0 × 10^{-3} M $[Fe(CN)_6]^{4-}$ solution prepared in lithium perchlorate, after incubation in increasing concentrations of CAP standard solutions.

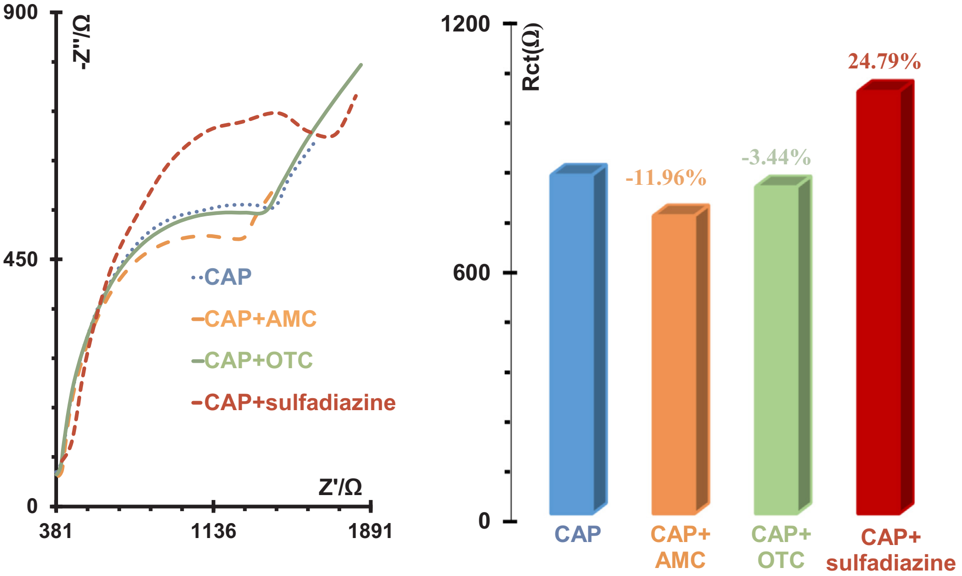

Fig. 6. Selectivity behaviour of the biosensor for CAP (1.00×10^{-6} M) against OTC (1.00×10^{-6} M), AMC (1.00×10^{-6} M) and sulfadiazine (1.00×10^{-6} M), after 20 min incubation.

(RSD) produced by each interfering species. The RSD for OTC was − 3.44%; for AMC − 11.96%; and for sulfadiazine + 24.79%. While OTC and AMC had no significant interfering effect upon the CAP response, sulfadiazine reduced the analytical signal higher than 24%. Apparently, the interference of sulfadiazine was significant, but, as shown in the previously published work (Cardoso et al., 2018), this interference effect had nothing to do with the sensing surface, but reflected a chemical interaction between sulfadiazine and CAP. Overall, this data shows a similar performance to the commercial C-SPEs, thereby confirming the good selectivity of the LIG devices.

Also, the storage stability of the biosensor was evaluated by letting stand a ready-to-use device for one week. After this period, the device was calibrated and the changes in the main analytical features showed a linear behaviour between 100 nM and 10 mM and LOD was 12.8 nM. Comparing these analytical features (Fig. S4) to the ready-to-use device, it was possible to see that linearity and LOD properties were partially lost, however the sensor device had a good slope comparing with the commercial G-SPE.

4. Conclusions

The work described herein shows for the first time the combination of a simple and reproducible carbon-electrode fabrication by laser irradiation of polyimide substrates, with the on-site assembly of a biorecognition element made by molecular imprinting technology. The carbon material so produced is constituted by graphene and the resulting 3-electrode system compared favourably to commercial devices in terms of sensitivity and linear response range. The LIG biosensor showed high sensitivity against CAP, being able to detect very low concentrations of CAP, down to the nanomolar range. It also showed a good selectivity against other possible interfering antibiotics (OTC, AMC, and sulfadiazine).

Besides the advantages in terms of analytical features, the LIG biosensor allows an easy redesign of the electrode-system, to other shapes and forms, following the current needs of the scientific community. Moreover, the devices proposed herein are constructed by a one-step mask-free approach, which is a scalable method for massive biosensor platforms production. The biorecognition element is also assembled by an on-site process, thereby facilitating the scalability of this specific biosensor.

Overall, the strategy proposed herein in terms of 3-electrode system and its combination to a suitable biorecognition element is considered a promising approach for the future of on-site analysis in different contexts, including environment, industrial and health applications. Moreover, this platform can be easily adopted for multi-detections systems to measure relevant molecules at the same time.

Acknowledgements

The authors acknowledge funding from project PTDC/AAG-TEC/5400/2014, POCI-01-0145-FEDER-016637 and POCI-01-0145-FEDER-007688, UID/CTM/50025/2013 funded by European funds, through FEDER (European Funding or Regional Development) via COMPETE2020 – POCI (operational program for internationalization and competitively) and by national funding through the Fundação para a Ciência e Tecnologia, I.P., Portugal (FCT-MCTES). ARC, ACM and AFC also acknowledge funding to National Foundation for Science and Technology, I.P., Portugal (FCT-MCTES) through the Ph.D. Grant SFRH/BD/130107/2017, SFRH/BD/115173/2016 and DAEPHYS-FCT PD/BD/114063/2015, respectively. AFC also acknowledges the funding from "Programa de Estímulo à Investigação 2016" from Fundação Calouste Gulbenkian.

Appendix A. Supplementary material

Supplementary data associated with this article can be found in the online version at doi:10.1016/j.bios.2018.10.015.

References

Abnous, K., Danesh, N.M., Ramezani, M., Emrani, A.S., Taghdisi, S.M., 2016. A novel colorimetric sandwich aptasensor based on an indirect competitive enzyme-free method for ultrasensitive detection of chloramphenicol. Biosens. Bioelectron. 78, 80–86. https://doi.org/10.1016/j.bios.2015.11.028.

Arduini, F., Micheli, L., Moscone, D., Palleschi, G., Piermarini, S., Ricci, F., Volpe, G., 2016. Electrochemical biosensors based on nanomodified screen-printed electrodes: recent applications in clinical analysis. TrAC – Trends Anal. Chem. 79, 114–126. https://doi.org/10.1016/j.trac.2016.01.032.

Ashwin, H.M., Stead, S.L., Taylor, J.C., Startin, J.R., Richmond, S.F., Homer, V., Bigwood, T., Sharman, M., 2005. Development and validation of screening and confirmatory methods for the detection of chloramphenicol and chloramphenicol glucuronide using SPR biosensor and liquid chromatography-tandem mass spectrometry. Anal. Chim. Acta 529, 103–108. https://doi.org/10.1016/j.aca.2004.08.035.

Bernalte, E., Foster, C.W., Brownson, D.A.C., Mosna, M., Smith, G.C., Banks, C.E., 2016. Pencil it in: exploring the feasibility of hand-drawn pencil electrochemical sensors and their direct comparison to screen-printed electrodes. Biosensors 6. https://doi.

org/10.3390/bios6030045.

Cai, J., Lv, C., Watanabe, A., 2016. Cost-effective fabrication of high-performance flexible all-solid-state carbon micro-supercapacitors by blue-violet laser direct writing and further surface treatment. J. Mater. Chem. A 4, 1671–1679. https://doi.org/10.1039/C5TA09450J.

Cardoso, A.R., Tavares, A.P.M., Sales, M.G.F., 2018. In-situ generated molecularly imprinted material for chloramphenicol electrochemical sensing in waters down to the nanomolar level. Sens. Actuators B Chem. 256, 420–428. https://doi.org/10.1016/J.SNB.2017.10.114.

Carvalho, A.F., Holz, T., Santos, N.F., Ferro, M.C., Martins, M.A., Fernandes, A.J.S., Silva, R.F., Costa, F.M., 2016. Simultaneous CVD synthesis of graphene-diamond hybrid films. Carbon 98, 99–105. https://doi.org/10.1016/j.carbon.2015.10.095.

Chang, T.L., Chen, Z.C., Tseng, S.F., 2016. Laser micromachining of screen-printed graphene for forming electrode structures. Appl. Surf. Sci. 374, 305–311. https://doi.org/10.1016/j.apsusc.2015.12.031.

Chyan, Y., Ye, R., Li, Y., Singh, S.P., Arnusch, C.J., Tour, J.M., 2018. Laser-induced graphene by multiple lasing: toward electronics on cloth, paper, and food. ACS Nano. https://doi.org/10.1021/acsnano.7b08539.

El-Kady, M.F., Strong, V., Dubin, S., Kaner, R.B., 2012. Laser scribing of high-performance and flexible graphene-based electrochemical capacitors. Science (80-) 335, 1326–1330. https://doi.org/10.1126/science.1216744.

Fang, Y., Hester, J.G.D., Su, W., Chow, J.H., Sitaraman, S.K., Tentzeris, M.M., 2016. A bio-enabled maximally mild layer-by-layer Kapton surface modification approach for the fabrication of all-inkjet-printed flexible electronic devices. Nat. Publ. Gr. 1–9. https://doi.org/10.1038/srep39909.

Fenzl, C., Nayak, P., Hirsch, T., Otto, S., Alshareef, H.N., Baeumner, A.J., 2017. laser-scribed graphene electrodes for aptamer-based biosensing laser-scribed graphene electrodes for aptamer-based biosensing. ACS Sens.

Ferrari, A.C., Basko, D.M., 2013. Raman spectroscopy as a versatile tool for studying the properties of graphene. Nat. Nanotechnol. 8, 235–246. https://doi.org/10.1038/nnano.2013.46.

Hayat, A., Marty, J.L., 2014. Disposable screen printed electrochemical sensors: tools for environmental monitoring. Sensors 14, 10432–10453. https://doi.org/10.3390/s140610432.

Hughes, G., Westmacott, K., Honeychurch, K.C., Crew, A., Pemberton, R.M., Hart, J.P., 2016. Recent advances in the fabrication and application of screen-printed electrochemical (bio)sensors based on carbon materials for biomedical, agri-food and environmental analyses. Biosensors 6. https://doi.org/10.3390/bios6040050.

In, J. Bin, Hsia, B., Yoo, J.-H., Seungmin, Hyun, Carraro, Carlo, Roya Maboudian, C.P.G.,, 2015. Facile fabrication of flexible all solid-state micro-supercapacitor by direct laser writing of porous carbon in polyimide. Carbon 83, 144–151.

Khan, M.A.R., Moreira, T.C., Riu, F., Sales, J., F., G, M., 2016. Plastic antibody for the electrochemical detection of bacterial surface proteins. Sens. Actuators B Chem. 233, 697–704. https://doi.org/10.1016/j.snb.2016.04.075.

Kim, Y.-J., Kim, Y., Novoselov, K., Hong, B.H., 2015. Engineering electrical properties of graphene: chemical approaches. 2D Mater. 2, 042001. https://doi.org/10.1088/2053-1583/2/4/042001.

Kumar, S., Ahlawat, W., Kumar, R., Dilbaghi, N., 2015. Graphene, carbon nanotubes, zinc oxide and gold as elite nanomaterials for fabrication of biosensors for healthcare. Biosens. Bioelectron. 70, 498–503. https://doi.org/10.1016/j.bios.2015.03.062.

Li, W., Tan, C., Lowe, M.A., Abruña, H.D., Ralph, D.C., 2011. Electrochemistry of individual monolayer graphene sheets. ACS Nano 5, 2264–2270. https://doi.org/10.1021/nn103537q.

Lin, J., Peng, Z., Liu, Y., Ruiz-Zepeda, F., Ye, R., Samuel, E.L.G., Yacaman, M.J., Yakobson, B.I., Tour, J.M., 2014. Laser-induced porous graphene films from commercial polymers. Nat. Commun. 5, 1–8. https://doi.org/10.1038/ncomms6714.

Luo, S., Hoang, P.T., Liu, T., 2016. Direct laser writing for creating porous graphitic structures and their use for flexible and highly sensitive sensor and sensor arrays. Carbon 96, 522–531. https://doi.org/10.1016/j.carbon.2015.09.076.

Ma, Y., Chen, Y., 2015. Three-dimensional graphene networks: synthesis, properties and applications. Natl. Sci. Rev. 2, 40–53.

Rackus, D.G., Shamsi, M.H., Wheeler, A.R., 2015. Electrochemistry, biosensors and microfluidics: a convergence of fields. Chem. Soc. Rev. 44, 5320–5340. https://doi.org/10.1039/C4CS00369A.

Ramnani, P., Saucedo, N.M., Mulchandani, A., 2016. Carbon nanomaterial-based electrochemical biosensors for label-free sensing of environmental pollutants. Chemosphere 143, 85–98. https://doi.org/10.1016/j.chemosphere.2015.04.063.

Rao, R., Podila, R., Tsuchikawa, R., Katoch, J., Tishler, D., Rao, A.M., Ishigami, M., 2011. Effects of layer stacking on the combination raman modes in graphene. ACS Nano 5, 1594–1599. https://doi.org/10.1021/nn1031017.

Samsonova, J.V., Cannavan, A., Elliott, C.T., 2012. A critical review of screening methods for the detection of chloramphenicol, thiamphenicol, and florfenicol residues in foodstuffs. Crit. Rev. Anal. Chem. 42, 50–78. https://doi.org/10.1080/10408347.2012.629951.

Song, Y., Luo, Y., Zhu, C., Li, H., Du, D., Lin, Y., 2016. Recent advances in electrochemical biosensors based on graphene two-dimensional nanomaterials. Biosens. Bioelectron. 76, 195–212. https://doi.org/10.1016/j.bios.2015.07.002.

Taleat, Z., Khoshroo, A., Mazloum-Ardakani, M., 2014. Screen-printed electrodes for biosensing: a review (2008–2013). Microchim. Acta 181, 865–891. https://doi.org/10.1007/s00604-014-1181-1.

Tehrani, F., Bavarian, B., 2016. Facile and scalable disposable sensor based on laser engraved graphene for electrochemical detection of glucose. Sci. Rep. 6, 27975. https://doi.org/10.1038/srep27975.

Trojanowicz, M., 2016. Impact of nanotechnology on design of advanced screen-printed electrodes for different analytical applications. TrAC – Trends Anal. Chem. 84, 22–47. https://doi.org/10.1016/j.trac.2016.03.027.

Xia, X., Xu, Y., Ke, R., Zhang, H., Zou, M., Yang, W., Li, Q., 2013. A highly sensitive europium nanoparticle-based lateral flow immunoassay for detection of chloramphenicol residue. Anal. Bioanal. Chem. 405, 7541–7544. https://doi.org/10.1007/s00216-013-7210-9.

Xu, G., Jarjes, Z.A., Desprez, V., Kilmartin, P.A., Travas-Sejdic, J., 2018. Sensitive, selective, disposable electrochemical dopamine sensor based on PEDOT-modified laser scribed graphene. Biosens. Bioelectron. 107, 184–191. https://doi.org/10.1016/j.bios.2018.02.031.

Xu, J., Wang, Y., Hu, S., 2017. Nanocomposites of graphene and graphene oxides: synthesis, molecular functionalization and application in electrochemical sensors and biosensors. A review. Microchim. Acta 184. https://doi.org/10.1007/s00604-016-2007-0.

Yamanaka, K., Vestergaard, M.C., Tamiya, E., 2016. Printable electrochemical biosensors: a focus on screen-printed electrodes and their application. Sensors 16, 1–16. https://doi.org/10.3390/s16101761.

Yang, Y., Yin, D., Zhong, C., Xiong, R., Shi, J., Liu, Z., Wang, X., Lei, Q., 2013. Surface morphology and Raman analysis of the polyimide film aged under bipolar pulse voltage. Polym. Eng. Sci. 1–6. https://doi.org/10.1002/pen.

Ye, R., James, D.K., Tour, J.M., 2018. Laser-induced graphene. Acc. Chem. Res. 51, 1609–1620. https://doi.org/10.1021/acs.accounts.8b00084.

Yoo, E.-H., Lee, S.-Y., 2010. Glucose biosensors: an overview of use in clinical practice. Sensors 10, 4558–4576. https://doi.org/10.3390/s100504558.

Żelechowska, K., Kondratowicz, I., Sadowski, W., 2014. 3D porous graphene-based structures – synthesis and applications. Carbon Nanotechnol. 210–241.

Zheng, D., Hu, H., Liu, X., Hu, S., 2015. Application of graphene in electrochemical sensing. Curr. Opin. Colloid Interface Sci. 20, 383–405. https://doi.org/10.1016/j.cocis.2015.10.011.

Zhou, B., Zhang, J., Fan, J., Zhu, L., Zhang, Y., Jin, J., Huang, B., 2015. A new sensitive method for the detection of chloramphenicol in food using time-resolved fluoroimmunoassay. Eur. Food Res. Technol. 240, 619–625. https://doi.org/10.1007/s00217-014-2363-0.